Chinese Journal of
POLYMER SCIENCE

RESEARCH ARTICLE

https://doi.org/10.1007/s10118-023-2918-2
Chinese J. Polym. Sci. **2023**, *41*, 1215–1222

Regioregular Asymmetric Diketopyrrolopyrrole Copolymers with Good Molecular Ordered Assembly Ability for High-performance Polymer Transistors

Qing-Qing Liu[a,b,†], Jia-Xin Yang[a,b,†], Man Zhao[a], Can Gao[a*], Bo Guan[a,b*], and Huan-Li Dong[a,b*]

[a] *Beijing National Laboratory for Molecular Sciences, Key Laboratory of Organic Solids, Institute of Chemistry, Chinese Academy of Sciences, Beijing 100190, China*
[b] *School of Chemical Sciences, University of Chinese Academy of Sciences, Beijing 100049, China*

Electronic Supplementary Information

Abstract Introduction of asymmetric units into conjugated polymers is an important strategy to regulate the photophysical and electronic properties of polymers, as asymmetric units can not only regulate solubility and energy levels, but also molecular stacking and orientation, thus giving much higher optoelectronic properties. However, very few studies have been reported in this field. The semiconducting properties of conjugated polymers could be regulated through regioregularity adjustment. Here, we took the asymmetric thiophene/pyridine side group DPP as core and developed the regioregular monomer T-Py-DPP through three steps: alkyl chain introduction, tin monomer coupling and NBS double bromination. The T-Py-DPP monomer was polymerized into *reg*-PPyTDPP-2FBT with a head-to-head structure. The regioregularity of T-Py-DPP unit endowed *reg*-PPyTDPP-2FBT with backbone planarity, self-assembly orientation, network-like morphology and high crystallinity in films, thus the superior bipolar transport properties. The highest hole and electron mobilities of *reg*-PPyTDPP-2FBT were 0.93 and 0.57 $cm^2 \cdot V^{-1} \cdot s^{-1}$, respectively, with 40% improvement relative to the regiorandom polymer.

Keywords Asymmetric copolymers; Regioregularity; Good orientation; Organic field-effect transistor; Enhanced performance

Citation: Liu, Q. Q.; Yang, J. X.; Zhao, M.; Gao, C.; Guan, B.; Dong, H. L. Regioregular asymmetric diketopyrrolopyrrole copolymers with good molecular ordered assembly ability for high-performance polymer transistors. *Chinese J. Polym. Sci.* **2023**, *41*, 1215–1222.

INTRODUCTION

Conjugated polymers have attracted tremendous interest in the fabrication of printable, mechanical and portable electronic devices with high performance.[1–6] One of the advantages of conjugated polymers is that their unique physical properties can be easily tuned through structure modification to suit different application situations,[7–10] such as organic field-effect transistors (OFETs), organic light-emitting diodes (OLEDs), organic solar cells (OSCs) and organic light-emitting transistors (OLETs).[11–15] Much attention has been paid on developing advanced topological and rational chemical building blocks for both the core unit and substituents, in pursuit of novel conjugated polymers with superior device performances.[16–19] The introduction of asymmetric units into polymers is an important strategy for the control of photoelectric properties of polymers because the asymmetric building blocks could finely tune the solubility, energy level, molecular stacking and orientation of conjugated polymers.[20–22] To produce asymmetric conjugated polymers, three asymmetric factors are often adopted: (1) asymmetric conjugated backbone, (2) asymmetric alkyl chain, and (3) asymmetric halogen substituent, such as thiophene/pyridine flanked diketopyrrolopyrrole (T-Py-DPP),[23] *p*F-thiophene,[24] and asymmetric Si—O side chain.[25] The first asymmetric DPP polymers PDPPTT-2T and PDPPMT-2T were synthesized by substitution of thiophene and thieno[3,2-*b*]thiophene units (TT).[26] The disruption of the symmetry of the molecular mainchain resulted in a good solubility in toluene. The films of two polymers exhibited preferentially edge-on molecular packing with high crystallinity, which resulted in high hole mobilities for in plane transport. In addition to substitute the DPP unit with dual electron donors, researchers also tried to replace one substituent with the electron-withdrawing groups, in hoping of adjusting the electron deficiency of building blocks. Pyridine is an effective electron deficient aromatic ring that can be used as the flanker. The asymmetric T-Py-DPP units in polymers PPyTDPP-TT and PPyTDPP-BT showed deep-lying HOMO energy levels (−5.28 and −5.14 eV) and narrow bandgaps (~1.5 eV) due to the electron-deficient pyridine units.[23] It also indicates that modifying conjugated polymers with asymmetric substituents have advantages of chemical structure diversity

* Corresponding authors, E-mail: cangao@iccas.ac.cn (C.G.)
E-mail: guanbo@iccas.ac.cn (B.G.)
E-mail: dhl522@iccas.ac.cn (H.L.D.)

† These authors contributed equally to this work.

Received October 28, 2022; Accepted December 1, 2022; Published online February 1, 2023

and good adjustability in photoelectrical properties, and stronger intermolecular binding energy and larger dipole moment than symmetric conjugated polymers.[26,27]

However, the introduction of asymmetric units in polymers, also brings the issue of regioregularity, which is mainly due to the indeterminate structures in the mainchain of the polymer may result in disordered electron distribution, unfavorable backbone geometry, unanticipated intermolecular stacking, and thus decreasing the optoelectronic performances of the polymers.[28–30] Some asymmetric polymers with regioregular structures were demonstrated to be superior in terms of mobility and solar cell performance.[31,32] For example, poly(3-hexylthiophene) (P3HT) batches with a high degree of regioregularity (head-to-tail) have shown higher levels of crystallinity, edge-on orientation and higher mobility (0.1 $cm^2 \cdot V^{-1} \cdot s^{-1}$) when compared to batches with a lower degree of backbone regularity (<10^{-5} $cm^2 \cdot V^{-1} \cdot s^{-1}$).[33,34] Regioregular asymmetric conjugated polymers exhibited better π-stacking than their regiorandom counterparts. Bazan and co-workers synthesized regioregular polymers CDTPT containing pyridyl[2,1,3]thiadiazole (PT) units. Compared to their regiorandom counterparts, the regioregular polymers exhibited a hole mobility of 2 magnitude orders of increase.[35,36] The high mobilities were realized when the polymer chains were organized within crystalline fibers and the charge migration predominately occurred along the direction of the fiber. These results encourage us to further explore the influence of regioregularity that has strictly confined monomeric units along the polymer backbone.

Based on our previous research,[37,38] the regioregular asymmetric T-Py-DPP based copolymers are designed and synthesized *via* direct arylation polycondensation (Fig. 1a). A novel D-A type conjugated copolymer *reg*-PPyTDPP-2FBT with regioregular backbone is more favourable for the formation of planar structures than regiorandom *ran*-PPyTDPP-2FBT. This structural feature originates from the exclusive regioselectivity at the asymmetric thiophene/pyridine flanked DPP, and the preferential chemoselectivity to form a "weak donor-strong acceptor" segment during polymerization. *Reg*-PPyTDPP-2FBT exhibits "head-to-head" configuration and displays a fibrous-network with an average fiber, while *ran*-PPyTDPP-2FBT presents a rather amorphous morphology without evident texture. *Reg*-PPyTDPP-2FBT is demonstrated that regioregular polymer with enhanced solid-state packing order, which results in a significant increase in charge-transporting than that of regiorandom polymers.[29,39]

EXPERIMENTAL

General Considerations

All chemicals are commercially available and are used without further treatment unless otherwise specifically stated. The synthesis and characterization of the nuclear magnetic resonance (NMR), high-resolution MALDI Fourier transform ion cyclotron resonance mass spectrometry (HR-MALDI-FT-ICR), absorption spectra measurement, ultraviolet photoelectron spectroscopy (UPS) spectra, thermogravimetric analysis (TGA), gel permeation chromatography (GPC), the preparation and characterization of monomers and polymers, OFET characteristics, atomic force microscopy (AFM) measurement, grazing incident X-ray diffraction (GIXRD) measurement are provided in detail in the Supporting Information.

RESULTS AND DISCUSSION

Synthesis and Characterization of *reg*-PPyTDPP-2FBT

The synthesis of *reg*-PPyTDPP-2FBT is illustrated in Fig. 1(b). To avoid the structural regiorandom arising from the discrepancy in the reaction activity of the asymmetric compound T-Py-DPP unit, a symmetric A-D-A type intermediate compound, 6,6'-((3,3'-difluoro-[2,2'-bithiophene]-5,5'-diyl)bis(pyridine-5,2-diyl))bis(3-(5-bromothiophen-2-yl)-2,5-dialkyl-2,5-dihy-

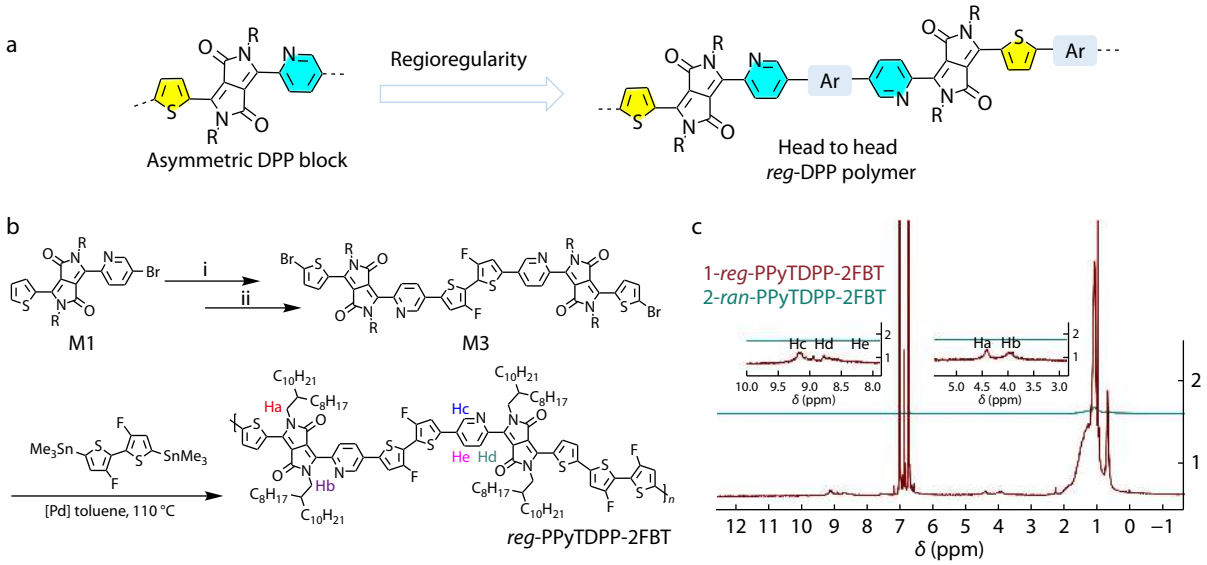

Fig. 1 (a) Illustration of the design concept of regioregular asymmetric DPP polymers arranged head to head; (b) Synthetic route to *reg*-PPyTDPP-2FBT; (c) High temperature ^{1}H-NMR spectra of *reg*-PPyTDPP-2FBT and *ran*-PPyTDPP-2FBT (90 °C in 1,1,2,2-tetrachloroethane-d_2).

https://doi.org/10.1007/s10118-023-2918-2

dropyrrolo[3,4-*c*]pyrrole-1,4-dione) (M3), was synthesized as a macromonomer. The synthesis was carried out using a 3-(5-bromopyridin-2-yl)-2,5-dialkyl-6-(thiophen-2-yl)-2,5-dihydropyrrolo[3,4-c]pyrrole-1,4-dione (M1) and (3,3'-difluoro-[2,2'-bithiophene]-5,5'-diyl)bis(trimethylstannane) (Sn-2F-bithiophene) as the starting materials in a palladium-catalyst coupling reaction and subsequent bromination with *N*-bromosuccinimide. The target copolymer *reg*-PPyTDPP-2FBT was synthesized by Stille coupling polymerization using the dibromo-monomer M3 and Sn-2F-bithiophene as monomers. *ran*-PPyTDPP-2FBT as reference polymer was prepared by one-pot polymerization as comparison polymer based on our previous work.[37] The copolymers were purified by Soxhlet extraction by successively using the eluent of methanol, acetone, hexane and chloroform (the detailed synthetic routes are shown in Fig. S1 in the electronic supplementary information, ESI). The copolymers were precipitated in methanol from trichloromethane solution. The number-average molecular weight (M_n) of *reg*-PPyTDPP-2FBT and *ran*-PPyTDPP-2FBT are estimated as 26.9 kDa (dispersity, PDI=2.71) and 60.1 kDa (dispersity, PDI=2.64), as evaluated by high-temperature gel permeation chromatography measurement using 1,2,4-trichlorobenzene as the eluent, and the linear polystyrene as the standard (Fig. S2 in ESI and Table 1). The structure of conjugated chain of the regioregular copolymer *reg*-PPyTDPP-2FBT is determined (head-to-head), and its characteristic H atom peaks, such as H_a, H_b, H_c, H_d and H_e, are enhanced by the superposition of the characteristic peaks in the aromatic region, as shown in Fig. 1(c). Due to the random orientation of asymmetric DPP units within the single conjugated chain of *ran*-PPyTDPP-2FBT (head-to-head, head-to-tail or tail-to-tail), the chemical environment of H atoms in the aromatic region are different. The H shift in the NMR spectra is different. Thus, peaks in the aromatic region of the regiorandom copolymer *ran*-PPyTDPP-2FBT are relatively weak. It indicates that the *reg*-PPyTDPP-2FBT was regioregular within conjugated chains. *Reg*-PPyTDPP-2FBT is thermally stable with decomposition temperatures of 390 °C (T_d, weight loss of 5%), as stable as *ran*-PPyTDPP-2FBT (Fig. S3 in ESI). The UV-Vis absorption spectra of *reg*-PPyTDPP-2FBT and *ran*-PPyTDPP-2FBT solution and thin film are shown in Fig. S4 (in ESI). The short wavelength band around 440 nm is attributable to localized π-π^* transitions, and the long wavelength band around 750 nm is related to intramolecular charge-transfer effect (ICT) between the weak donor moiety and the asymmetric T-Py-DPP moiety. The absorption spectra of *reg*-PPyTDPP-2FBT and *ran*-PPyTDPP-2FBT in diluted trichloromethane have similar absorption peaks, with no red shift observed (Fig. S4a in ESI). While the absorption spectrum of *reg*-PPyTDPP-2FBT film exhibits about 20 nm red-shift relative to *ran*-PPyTDPP-2FBT, indicating an aggregation in *reg*-PPyTDPP-2FBT film due to strong intermolecular interactions between conjugated chains (Fig. S4b in ESI). The optical bandgaps of *reg*-PPyTDPP-2FBT and *ran*-PPyTDPP-2FBT were obtained from the onset absorptions of thin films, which are 1.43 and 1.51 eV, respectively. UPS spectra measurement was utilized to probe the electrochemical properties of the copolymers, with the corresponding characteristics shown in Fig. S5 (in ESI). The highest occupied molecular orbital (HOMO) energy levels of spin-cast *reg*-PPyTDPP-2FBT and *ran*-PPyTDPP-2FBT thin films determined by UPS are −5.17 and −5.34 eV, respectively. The lowest unoccupied molecular orbital (LUMO) energy levels of *reg*-PPyTDPP-2FBT and *ran*-PPyTDPP-2FBT are −3.74 and −3.88 eV indirectly obtained utilizing the HOMO level and optical bandgap (Table 1). The slightly raised HOMO level for *reg*-PPyTDPP-2FBT could be attributed to the more regioregular asymmetric T-Py-DPP orientation, which would improve the HOMO wave function delocalization along the polymer main chain.[40]

Aggregation Behaviors and Morphologies

To further explore the various aggregation behaviors and morphologies of *reg*-PPyTDPP-2FBT and *ran*-PPyTDPP-2FBT thin films, UV-Vis absorption spectra and AFM images under series temperature were carefully and simultaneously performed. Temperature-dependent UV-Vis absorption spectra of *reg*-PPyTDPP-2FBT and *ran*-PPyTDPP-2FBT show a remarkable blue-shift when the solution temperature increased from 30 °C to 100 °C (Figs. 2a–2c). At elevated temperature, these two polymers were well dissolved in 1,2-dichlorobenzene (*o*-DCB) and disaggregated. Maximum absorption band A_0 and its shoulder absorption band A_1 are corresponding to the aggregation and well-dissolved states, respectively. Based on the UV-Vis absorption features, the intensity ratio (A_0/A_1) at low-energy characteristic absorption bands was inferred to indicate the dissolution features when the temperature changed. With the temperature increasing, the A_0/A_1 ratios of *reg*-PPyTDPP-2FBT decreases more quickly than *ran*-PPyTDPP-2FBT, illustrating that regioregular polymer chain adopted the extended conformation in solution (insert diagrams) and the dissolution of *reg*-PPyTDPP-2FBT aggregates is much easier than that of *ran*-PPyTDPP-2FBT (Fig. 2c).[41] This indicates that the regioregular polymer *reg*-PPyTDPP-2FBT has a higher degree of aligned aggregation than the regiorandom *ran*-PPyTDPP-2FBT. In addition, the surface morphologies of such films were investigated by tapping mode atomic force microscopy (AFM). As shown in Figs. 2(d)–2(f), with thermal annealing temperature increasing, regioregular polymer *reg*-PPyTDPP-2FBT films prefers to self-assemble into ordered aggregates and displays fibrous-network, while *ran*-PPyTDPP-2FBT presents a rather amorphous morphology without evident texture (Fig. S4 in ESI). The AFM characterizations indicate that polymer *ran*-PPyTDPP-2FBT film morphology did not exhibit distinct variation upon thermal treatment at various temperatures. With the temperature increasing, the roughness of *reg*-PPyTDPP-2FBT film increased significantly relative to *ran*-PPyTDPP-2FBT, with a

Table 1 Summarized optical and electrochemical data.

Polymer	M_n (kDa)	PDI	$\lambda_{max\ sol}$ (nm)	$\lambda_{max\ film}$ (nm)	E_g^{opt} [a] (eV)	HOMO [b] (eV)	LUMO [c] (eV)
reg-PPyTDPP-2FBT	26.9	2.71	746	755	1.43	−5.17	−3.74
ran-PPyTDPP-2FBT	60.1	2.64	737	740	1.51	−5.39	−3.88

[a] Calculated from the solid absorption onsets according to $E_g^{opt} = 1240/\lambda_{onset}$; [b] HOMO levels were obtained by UPS; [c] Calculated energy levels of *reg*-PPyTDPP-2FBT and *ran*-PPyTDPP-2FBT.

https://doi.org/10.1007/s10118-023-2918-2

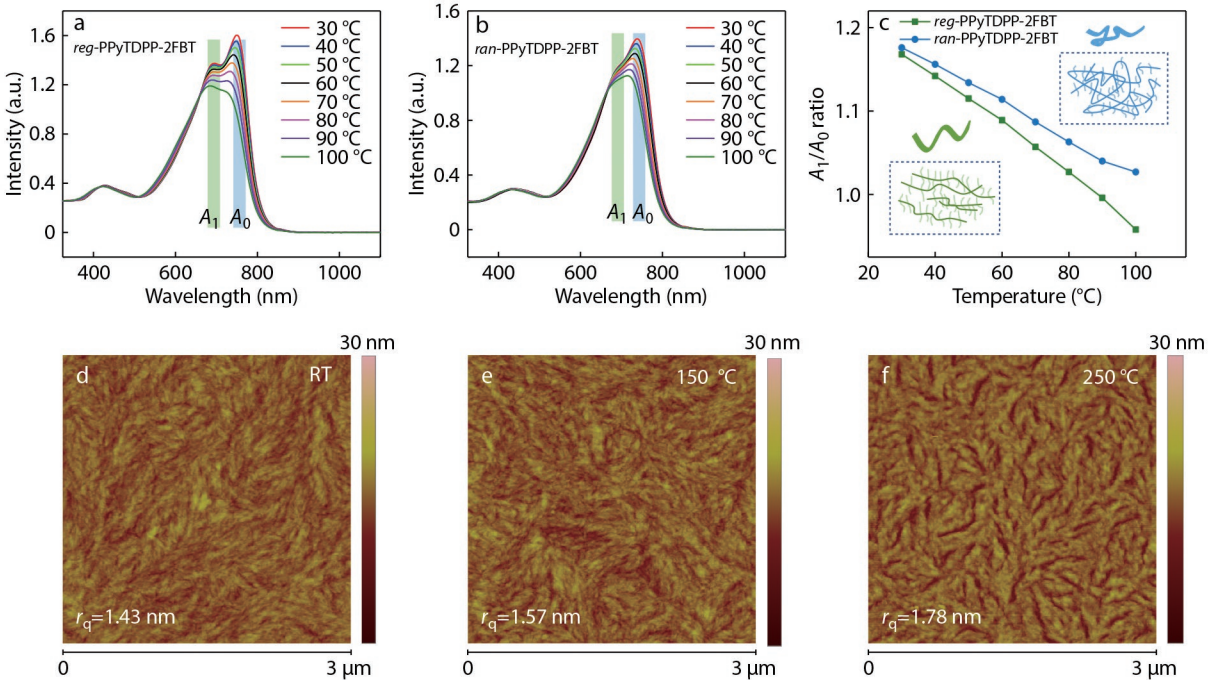

Fig. 2 Temperature-dependent absorption spectra of *reg*-PPyTDPP-2FBT (a) and *ran*-PPyTDPP-2FBT (b) in 1,2-dichlorobenzene (0.02 mg·mL^{-1}); (c) A_0/A_1 ratio of two polymers extracted from varied temperature UV-Vis spectra (the insert diagrams present the aggregation structure and internal chain conformation in the aggregates in solution); (d–f) AFM height images of *reg*-PPyTDPP-2FBT thin films annealed at different temperatures.

r_q value of 1.78 nm, suggesting that the structural regioregularity of *reg*-PPyTDPP-2FBT is conducive to obtain significantly aligned fibers for charge transport in semiconductor films.

Crystallinity and Molecular Orientation Behaviors

The molecular microstructures in thin films of *reg*-PPyTDPP-2FBT (Figs. 3a–3f) and *ran*-PPyTDPP-2FBT (Fig. S7 in ESI) at various thermal annealing temperatures was investigated by GIXRD. The coherence length (L_C) is a parameter to quantify the degree of copolymer crystalline order range, which can be calculated *via* Scherrer equation ($L_C = k \times 2\pi/\text{fwhm}$, where fwhm represents the full-width half-maximum of a diffraction peak).[42] Both copolymers (pristine films) exhibited a succession of (*h*00) peaks and *π*-*π* stacking peaks in the out-of plane (q_z) direction, suggesting that a mixed texture of face-on and edge-on orientation in thin films. With the increase of thermal annealing temperature, the crystalline features of both copolymers become sharper with increased L_C. Obvious diffraction peak (010) along the out-of-plane (q_{xy}) direction was observed of *reg*-PPyTDPP-2FBT annealed at 150 and 250 °C, indicating the edge-on dominated orientation relative to the substrate (Fig. 3g).[41,43] A distinct strong in-plane diffraction peak (010) was observed at q_{xy}=1.79 Å^{-1} (*d*-spacing of 0.35 nm), which was assigned to the *π*-*π* stacking distance (Table 2). The first-order lamellar stacking peak of *reg*-PPyTDPP-2FBT and *ran*-PPyTDPP-2FBT were observed at the almost same position (1.26 and 1.23 Å^{-1}), giving the same alkyl stacking distance of ~2.0 nm. For (010) diffraction peak, the maximum L_C of *reg*-PPyTDPP-2FBT was 6.0 nm, larger than *ran*-PPyTDPP-2FBT (5.1 nm), implying a longer crystalline order range. To conclude, regioregular copolymer *reg*-PPyTDPP-2FBT displayed higher degree of lamellar packing, denser interchain interactions and notably larger crystalline sizes to contribute to a higher efficient charge transport than *ran*-PPyTDPP-2FBT. Besides, the *reg*-PPyTDPP-2FBT can be assembled into nanowires with sharp diffraction patterns (Fig. S8 in ESI).

The planarity of the conjugated copolymer backbone has a great influence on charge transport properties. To understand the backbone geometry and the distribution of molecular orbitals, we carried out the density functional theory calculation at the B3LYP/6-31G(d,p) level. To simplify the calculation, the alkyl chains in the modeling dimer compound of *reg*-PPyTDPP-2FBT repeating unit were truncated as methyl groups. The HOMO and LUMO of *reg*-PPyTDPP-2FBT copolymer were delocalized along the molecular backbone on one repeating unit (Fig. S9 in ESI). The optimized geometries of the copolymer were nearly coplanar, as shown in Fig. 3(c). The dihedral angle (1.99°) between two repeating units in isomers and the twist angle (0.19°) between the F-thiophene units were smaller than those of the regiorandom copolymer *ran*-PPyTDPP-2FBT (4.24° and 0.9°, respectively).[37] The regioregular asymmetric T-Py-DPP moiety induced better planarity and promoted *π*-*π* stacking. It predicted better charge mobility properties of the regioregular polymer. The planar backbone of *reg*-PPyTDPP-2FBT resulted in a red-shift of the absorption and a narrower bandgap. These findings were in agreement with the absorption spectra and electrochemical studies discussed above.

Organic Field-Effect Transistors

To investigate the semiconducting properties of *reg*-PPyTDPP-2FBT, solution-processable OFET devices with TGBC (top-gate bottom-contact) configurations were fabricated using a

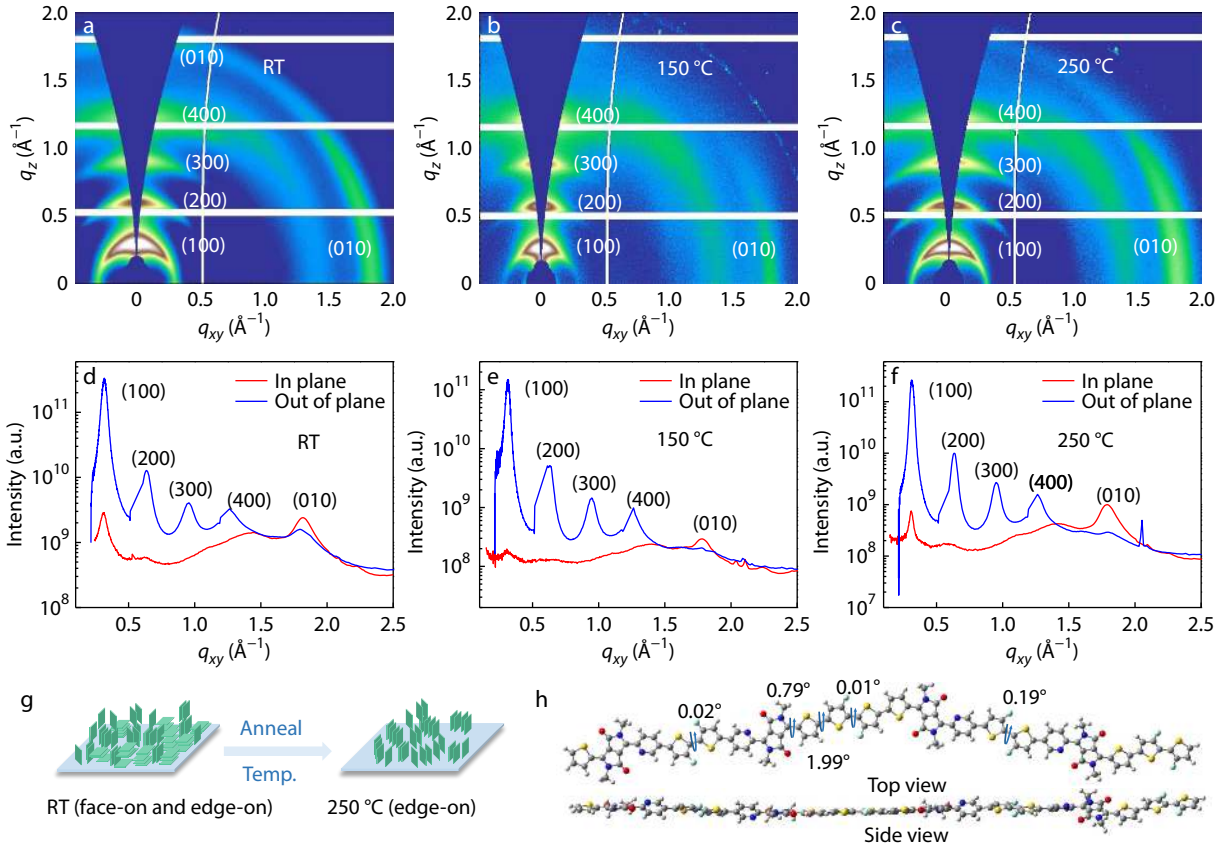

Fig. 3 2D-GIXRD images (a–c) and 1D-GIXRD of out-of-plane and in-plane line-cut profiles (d–f) of *reg*-PPyTDPP-2FBT thin films annealed at different temperatures; (g) Schematic illustration of *reg*-PPyTDPP-2FBT from mixed to a predominantly edge-on orientation with increasing annealing temperature; (h) Theoretical calculations of backbone coplanarity of dimer *reg*-PPyTDPP-2FBT repeat units (alkyl chains were replaced by methyl groups to simplify the calculation).

Table 2 Relevant crystallographic parameters of two polymer films.

Polymer	Temp. (°C)	π-π Spacing (nm)	In-plane fwhm (Å^{-1})	Lamellar spacing [a] (nm)	In-plane L_C (nm)
reg-PPyTDPP-2FBT	RT	0.35	0.13	1.96	4.6
	150	0.35	0.11	2.03	5.1
	250	0.35	0.09	2.03	6.0
ran-PPyTDPP-2FBT	RT	0.35	0.16	1.90	3.5
	150	0.35	0.14	1.96	3.5
	250	0.35	0.11	1.96	5.1

[a] Interlamellar distance calculated from the (100) peaks in the in-plane direction.

glass/Au/polymer/PMMA/Au architecture and were measured in glovebox (in ESI). We explored the charge transport properties of the regioregular polymer *reg*-PPyTDPP-2FBT, compared with regiorandom copolymer *ran*-PPyTDPP-2FBT at different thermal annealing temperatures (150 and 250 °C). Fig. 4 showed the transfer and output curves for the TGBC devices with *reg*-PPyTDPP-2FBT films after thermal annealing at 250 °C. *Reg*-PPyTDPP-2FBT clearly exhibited ambipolar charge transport behaviors. The charge mobilities (μ_e and μ_h), on/off current ratios (I_{on}/I_{off}), and threshold voltages (V_T) of OFETs are listed in Table S1. The average/highest μ_h and μ_e of *reg*-PPyTDPP-2FBT were 0.73/0.93 and 0.45/0.57 cm^2·V^{-1}·s^{-1}, respectively. Similarly, the average/highest μ_h and μ_e of *ran*-PPyTDPP-2FBT were 0.45/0.57 and 0.32/0.37 cm^2·V^{-1}·s^{-1}, respectively, after fitting the respective transfer curves (Fig. S10 in ESI). The OFETs with *reg*-PPyTDPP-2FBT thin films showed higher mobility and lower threshold voltages than that of *ran*-PPyTDPP-2FBT. In contrast, the mobility of *reg*-PPyTDPP-2FBT and *ran*-PPyTDPP-2FBT thin films after thermal annealing at 150 °C decreased significantly (Fig. S11 and Table S1 in ESI). The average/highest μ_h and μ_e of *reg*-PPyTDPP-2FBT were 0.46/0.59 and 0.19/0.25 cm^2·V^{-1}·s^{-1}, and that of *ran*-PPyTDPP-2FBT thin films were 0.40/0.52 and 0.15/0.21 cm^2·V^{-1}·s^{-1}, respectively. The charge transport characteristics of OFETs based on *reg*-PPyTDPP-2FBT and *ran*-PPyTDPP-2FBT thin films exhibited temperature dependence. The distribution of the mobility of two copolymers thin films annealed at optimal thermal annealing temperature 250 °C shown in Figs. 4(e) and 4(f), the average hole and electron mobility of *reg*-PPyTDPP-2FBT was 30%–40% higher than that of *ran*-PPyTDPP-2FBT. The high balanced and ambipolar mobilities of *reg*-PPyTDPP-2FBT might be due to regioregular copolymer higher degree of lamellar

https://doi.org/10.1007/s10118-023-2918-2

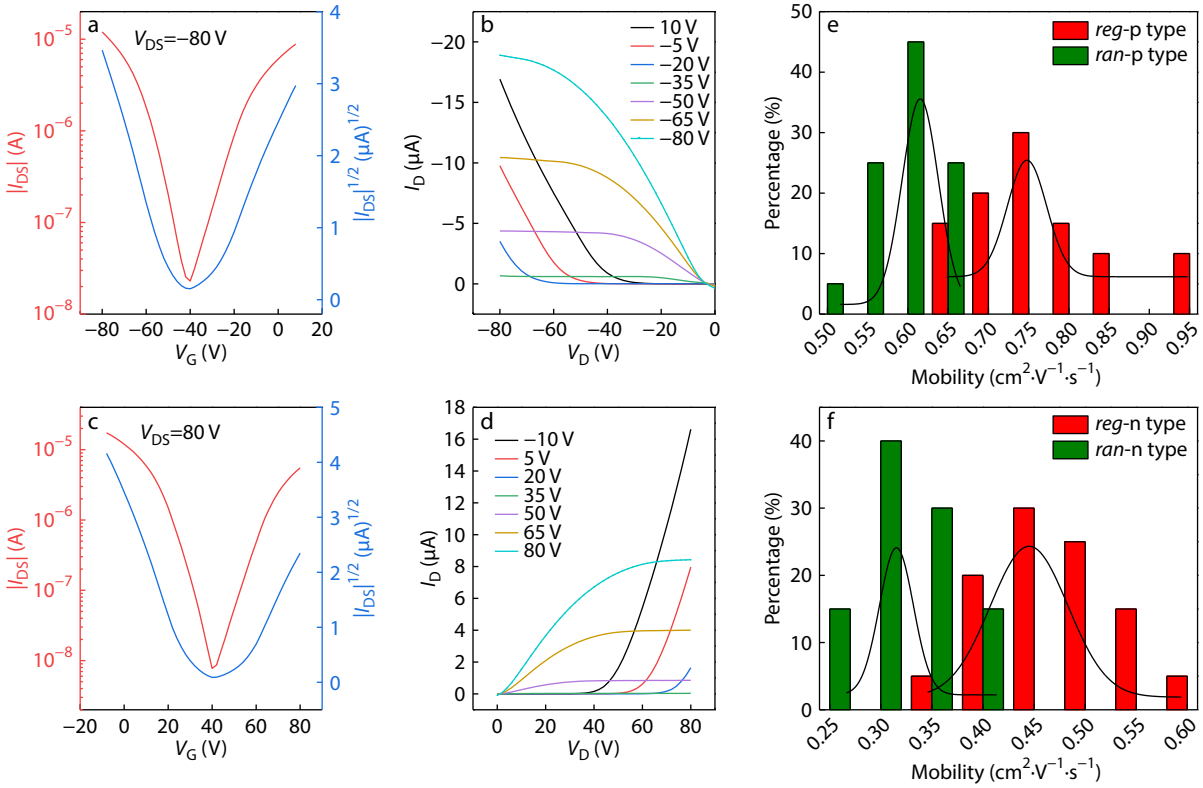

Fig. 4 Typical transfer (a, c) and output (b, d) curves obtained from OFET devices based on *reg*-PPyTDPP-2FBT thin films annealed at 250 °C; Mobility distribution of 20 numbers of p type (e) and n type (f) thin film OFET devices of *reg*-PPyTDPP-2FBT and *ran*-PPyTDPP-2FBT.

packing, denser interchain interactions and notably larger crystalline sizes than regiorandom copolymer to contribute to a higher efficient charge transport.

CONCLUSIONS

In conclusion, a new D-A type regioregular T-Py-DPP based conjugated copolymer *reg*-PPyTDPP-2FBT was designed and synthesized *via* direct arylation polycondensation, and fine regioselectivity symmetric intermediate compound M3 core was synthesized within two steps. With the introduction of regioregular asymmetric T-Py-DPP unit, regioregular *reg*-PPyTDPP-2FBT is more favorable for the formation of planar molecular backbone than regiorandom backbone polymer. *Reg*-PPyTDPP-2FBT films prefer to self-assemble into aggregates and display fibrous-network, higher degree of lamellar packing, denser interchain interactions and notably larger crystalline sizes. OFET based on *reg*-PPyTDPP-2FBT thin film exhibits remarkably enhanced hole and electron mobility with balanced feature, up to 0.93 and 0.57 cm^2·V^{-1}·s^{-1}, which are 30%–40% higher than that of *ran*-PPyTDPP-2FBT. Integrating asymmetric conjugated backbone framework with precisely defined T-Py-DPP unit orientations offers an effective molecular design strategy for the design of high-mobility conjugated polymers with self-assemble aggregates.

Conflict of Interests

The authors declare no interest conflict.

Electronic Supplementary Information

Electronic supplementary information (ESI) is available free of charge in the online version of this article at http://doi.org/10.1007/s10118-023-2918-2.

ACKNOWLEDGMENTS

This work was financially supported by the Ministry of Science and Technology of China (Nos. 2018YFA0703200 and 2022YFB3603800), the National Natural Science Foundation of China (Nos. 21875259, 52233010, 51725304, 61890943, 52103245 and 22021002), the CAS Project for Young Scientists in Basic Research (No. YSBR-053), the Youth Innovation Promotion Association of the Chinese Academy of Sciences, the National Program for Support of Top-notch Young Professionals, the Beijing National Laboratory for Molecular Sciences (No. BNLMS-CXXM-202012), and the Key Research Program of the Chinese Academy of Sciences (Nos. XDPB13 and 121111KYSB20200004).

REFERENCES

1 Luo, L.; Huang, W.; Yang, C.; Zhang, J.; Zhang, Q. Recent advances on π-conjugated polymers as active elements in high performance organic field-effect transistors. *Front. Phys.* **2021**, *16*, 33500.

2 Yao, Z. F.; Li, Q. Y.; Wu, H. T.; Ding, Y. F.; Wang, Z. Y.; Lu, Y.; Wang, J. Y.; Pei, J. Building crystal structures of conjugated polymers through X-ray diffraction and molecular modeling. *SmartMat*

2021, *2*, 378–387.
3 Zhou, Y.; Zhang, W.; Yu, G. Recent structural evolution of lactam- and imide-functionalized polymers applied in organic field-effect transistors and organic solar cells. *Chem. Sci.* **2021**, *12*, 6844–6878.
4 Adachi, C.; Sandanayaka, A. S. D. The leap from Organic light-emitting diodes to organic semiconductor laser diodes. *CCS Chem.* **2020**, *2*, 1203–1216.
5 He, M. N.; Zhao, Y.; Liu, Y. Q.; Wei, D. C. A 3D printable self-healing composite conductive polymer for sensitive temperature detection. *Chin. Chem. Lett.* **2020**, *31*, 826–830.
6 Yang, Y. Multi-tier computing networks for intelligent IoT. *Nat. Electron.* **2019**, *2*, 4–5.
7 Ni, Z. j.; Dong, H. L.; Wang, H. L.; Ding, S.; Zou, Y.; Zhao, Q.; Zhen, Y. G.; Liu, F.; Jiang, L.;Hu. W. P. Quinoline-flanked diketopyrrolopyrrole copolymers breaking through electron mobility over 6 cm^2 V^{-1} s^{-1} in flexible thin film devices. *Adv. Mater.* **2018**, *30*, 1704843.
8 Yang, J.; Wang, H.; Chen, J.; Huang, J.; Jiang, Y.; Zhang, J.; Shi, L.; Sun, Y.; Wei, Z.; Yu, G.; Guo, Y.; Wang, S.; Liu, Y. Bis-diketopyrrolopyrrole moiety as a promising building block to enable balanced ambipolar polymers for flexible transistors. *Adv. Mater.* **2017**, *29*, 1606162.
9 Yi, Z.; Wang, S.; Liu, Y. Design of high-mobility diketopyrrolopyrrole-*b* based *π*-conjugated copolymers for organic thin-film transistors. *Adv. Mater.* **2015**, *27*, 3589–3606.
10 Ma, J.; Tian, J.; Liu, Z.; Shi, D.; Zhang, X.; Zhang, G.; Zhang, D. Multi-stimuli-responsive field-effect transistor with conjugated polymer entailing spiropyran in the side chains. *CCS Chem.* **2020**, *2*, 632–641.
11 Xu, J.; Wang, S. H.; Wang, G. J. N.; Zhu, C. X.; Luo, S. C.; Jin, L. H.; Gu, X. D.; Chen, S. C.; Feig, V. R.; To, J. W. F.; Rondeau-Gagne, S.; Park, J.; Schroeder, B. C.; Lu, C.; Oh, J. Y.; Wang, Y. M.; Kim, Y. H.; Yan, H.; Sinclair, R.; Zhou, D. S.; Xue, G.; Murmann, B.; Linder, C.; Cai, W.; Tok, J. B. H.; Chung, J. W.; Bao, Z. N. Highly stretchable polymer semiconductor films through the nanoconfinement effect. *Science* **2017**, *355*, 59–64.
12 Qin, Z. S.; Gao, H. K.; Dong, H. L.; Hu, W. P. Organic light-emitting transistors entering a new development stage. *Adv. Mater.* **2021**, *33*, 2007149.
13 Huang, F; Bo, Z. S; Geng, Y. H.; Wang, X. H.; Wang, L. X.; Ma, Y. G.; Hou, J. H.; Hu, W. P.; Pei, J.; Dong, H. L.; Wang, S.; Li, Z; Shuai, Z. G.; Li, Y. F.; Cao, Y. Study on optoelectronic polymers: an overview and outlook. *Acta Polymerica Sinica* (in Chinese) **2019**, *50*, 988–1046.
14 Zhao, R. Y.; Liu, J.; Wang, L. X. Polymer acceptors containing B◊N units for organic photovoltaics. *Acc. Chem. Res.* **2020**, *53*, 1557–1567.
15 Yue, H.; Wang, Z.; Zhen, Y. Recent advances of self-healing electronic materials applied in organic field-effect transistors. *ACS Omega* **2022**, *7*, 18197–18205.
16 Miao, J.; Wang, Y.; Liu, J.; Wang, L. Organoboron molecules and polymers for organic solar cell applications. *Chem. Soc. Rev.* **2022**, *51*, 153–187.
17 Yao, Z. F.; Zheng, Y. Q.; Dou, J. H.; Lu, Y.; Ding, Y. F.; Ding, L.; Wang, J. Y.; Pei, J. Approaching crystal structure and high electron mobility in conjugated polymer crystals. *Adv. Mater.* **2021**, *33*, e2006794.
18 Yu, Z. D.; Lu, Y.; Wang, J. Y.; Pei, J. Conformation control of conjugated polymers. *Chemistry* **2020**, *26*, 16194–16205.
19 Wu, Y. J.; Zhao, Y.; Liu, Y. Q. Toward efficient charge transport of polymer-based organic field-effect transistors: molecular design, processing, and functional utilization. *Acc. Chem. Res.* **2021**, *2*, 1047–1058.
20 Wang, M.; Ford, M.; Phan, H.; Coughlin, J.; Nguyen, T. Q.; Bazan, G. C. Fluorine substitution influence on benzo[2,1,3]thiadiazole based polymers for field-effect transistor applications. *Chem. Commun.* **2016**, *52*, 3207–3210.
21 Yu, Y.; Wu, Y.; Zhang, A.; Li, C.; Tang, Z.; Ma, W.; Wu, Y.; Li, W. Diketopyrrolopyrrole polymers with thienyl and thiazolyl linkers for application in field-effect transistors and polymer solar cells. *ACS Appl. Mater. Interfaces* **2016**, *8*, 30328–30335.
22 Hu, D. P.; Chen, M.; Yang, Y. H.; Li, H. Y. Texture induced by molecular weight dispersity: polymorphism within poly(L-lactic acid) spherulites. *Chinese J. Polym. Sci.* **2020**, *38*, 1365–1373.
23 Qiu, G. G.; Ni, Z. J.; Wang, H. L.; Dong, H. L.; Zhang, J. Q.; Zhang, X. T.; Shu, Z. B.; Lu, K.; Zhen, Y. G.; Wei, Z. X.; Hu, W. P. Asymmetric thiophene/pyridine flanked diketopyrrolopyrrole polymers for high performance polymer ambipolar field-effect transistors and solar cells. *J. Mater. Chem. C* **2017**, *5*, 566–572.
24 Fan, B.; Li, M.; Zhang, D.; Zhong, W.; Ying, L.; Zeng, Z.; An, K.; Huang, Z.; Shi, L.; Bazan, G. C.; Huang, F.; Cao, Y. Tailoring regioisomeric structures of *π*-conjugated polymers containing monofluorinated *π*-bridges for highly efficient polymer solar cells. *ACS Energy Lett.* **2020**, *5*, 2087–2094.
25 Yen, H. C.; Lin, Y. C.; Chen, W. C. Modulation of the hydrophilicity on asymmetric side chains of isoindigo-based polymers for improving carrier mobility-stretchability properties. *Macromolecules* **2021**, *54*, 1665–1676.
26 Ji, Y.; Xiao, C.; Wang, Q.; Zhang, J.; Li, C.; Wu, Y.; Wei, Z.; Zhan, X.; Hu, W.; Wang, Z.; Janssen, R. A.; Li, W. Asymmetric diketopyrrolopyrrole conjugated polymers for field-effect transistors and polymer solar cells processed from a nonchlorinated solvent. *Adv. Mater.* **2016**, *28*, 943–950.
27 Gao, W.; Zhang, M.; Liu, T.; Ming, R.; An, Q.; Wu, K.; Xie, D.; Luo, Z.; Zhong, C.; Liu, F.; Zhang, F.; Yan, H.; Yang, C. Asymmetrical ladder-type donor-induced polar small molecule acceptor to promote fill factors approaching 77% for high-performance nonfullerene polymer solar cells. *Adv. Mater.* **2018**, *30*, 1800052.
28 Zhong, W.; Sun, S.; Ying, L.; Liu, F.; Lan, L.; Huang, F.; Cao, Y. High-performance organic field-effect transistors fabricated based on a novel ternary pi-conjugated copolymer. *ACS Appl. Mater. Interfaces* **2017**, *9*, 7315–7321.
29 Cho, Y.; Park, S.; Jeong, S.; Yang, H.; Lee, B.; Lee, S. M.; Lee, B. H.; Yang, C. Regioregular, yet ductile and amorphous indacenodithiophene-based polymers with high-mobility for stretchable plastic transistors. *J. Mater. Chem. C* **2021**, *9*, 9670–9682.
30 Huang, Y.; Zheng, N.; Wang, Z.; Ying, L.; Huang, F.; Cao, Y. Synthesis of regioregular *π*-conjugated polymers consisting of a lactam moiety *via* direct heteroarylation polymerization. *Chem. Commun.* **2017**, *53*, 1997–2000.
31 Leenaers, P. J.; van Eersel, H.; Li, J.; Wienk, M. M.; Janssen, R. A. J. Influence of regioregularity on the optoelectronic properties of conjugated diketopyrrolopyrrole polymers comprising asymmetric Monomers. *Macromolecules* **2020**, *53*, 7749–7758.
32 Zhong, H.; Li, C. Z.; Carpenter, J.; Ade, H.; Jen, A. K. Influence of regio- and chemoselectivity on the properties of fluoro-substituted thienothiophene and benzodithiophene copolymers. *J. Am. Chem. Soc.* **2015**, *137*, 7616–7619.
33 Kim, Y.; Cook, S.; Tuladhar, S. M.; Choulis, S. A.; Nelson, J.; Durrant, J. R.; Bradley, D. D. C.; Giles, M.; McCulloch, I.; Ha, C. S.; Ree, M. A strong regioregularity effect in self-organizing conjugated polymer films and high-efficiency polythiophene:fullerene solar cells. *Nat. Mater.* **2006**, *5*, 197–203.
34 Sirringhaus, H.; Brown, P. J.; Friend, R. H.; Nielsen, M. M.; Bechgaard, K.; Langeveld-Voss, B. M. W.; Spiering, A. J. H.; Janssen, R. A. J.; Meijer, E. W.; Herwig, P.; de Leeuw, D. M. Two-dimensional charge transport in self-organized, high-mobility conjugated polymers. *Nature* **1999**, *401*, 685–688.

https://doi.org/10.1007/s10118-023-2918-2

35 Coughlin, J. E.; Zhugayevych, A.; Wang, M.; Bazan, G. C.; Tretiak, S. Charge delocalization characteristics of regioregular high mobility polymers. *Chem. Sci.* **2017**, *8*, 1146–1151.
36 Perez, L. A.; Zalar, P.; Ying, L.; Schmidt, K.; Toney, M. F.; Nguyen, T. Q.; Bazan, G. C.; Kramer, E. J. Effect of backbone regioregularity on the structure and orientation of a donor-acceptor semiconducting copolymer. *Macromolecules* **2014**, *47*, 1403–1410.
37 Yang, J. X.; Liu, Q. Q.; Hu, M. X.; Ding, S.; Liu, J.; Wang, Y. S.; Liu, D.; Gao, H. K.; Hu, W. P.; Dong, H. L. Well-balanced ambipolar diketopyrrolopyrrole-based copolymers for OFETs, inverters and frequency doublers. *Sci. China Chem.* **2021**, *64*, 1410–1416.
38 Ding, S.; Ni, Z. J.; Hu, M. X.; Qiu, G. G.; Li, J.; Ye, J.; Zhang, X. T.; Liu, F.; Dong, H. L.; Hu, W. P. An asymmetric furan/thieno[3,2-*b*]thiophene diketopyrrolopyrrole building block for annealing-free green solvent processable organic thin-film transistors. *Macromol. Rapid Commun.* **2018**, *39*, 1800225.
39 Aoshima, K.; Nomura, M.; Saeki, A. Regioregularity and electron deficiency control of unsymmetric diketopyrrolopyrrole copolymers for organic photovoltaics. *ACS Omega* **2019**, *4*, 15645–15652.
40 Ying, L.; Hsu, B. B.; Zhan, H.; Welch, G. C.; Zalar, P.; Perez, L. A.; Kramer, E. J.; Nguyen, T. Q.; Heeger, A. J.; Wong, W. Y.; Bazan, G. C. Regioregular pyridal[2,1,3]thiadiazole π-conjugated copolymers. *J. Am. Chem. Soc.* **2011**, *133*, 18538–18541.
41 Wang, Z. Y.; Di Virgilio, L.; Yao, Z. F.; Yu, Z. D.; Wang, X. Y.; Zhou, Y. Y.; Li, Q. Y.; Lu, Y.; Zou, L.; Wang, H. I.; Wang, X. Y.; Wang, J. Y.; Pei, J. Correlating charge transport properties of conjugated polymers in solution aggregates and thin-film aggregates. *Angew. Chem. Int. Ed.* **2021**, *60*, 20483–20488.
42 Rivnay, J. M. S. C.; Miller, C. E.; Salleo, A.; Toney, M. F. Quantitative determination of organic semiconductor microstructure from the molecular to device scale. *Chem. Rev.* **2012**, *112*, 5488–5519.
43 Ni, Z. J; Wang, H. L.; Zhao, Q.; Zhang, J. Q.; Wei, Z. X.; Dong, H. L.; Hu, W. P. Ambipolar conjugated polymers with ultrahigh balanced hole and electron mobility for printed organic complementary logic *via* a two-step C-H activation strategy. *Adv. Mater.* **2019**, *31*, e1806010.

https://doi.org/10.1007/s10118-023-2918-2